Semi-analytical calculation of resonant modes in axially asymmetric microtube resonators

CrossMark

Yingwu Lan[a], Shilong Li[b], Zhongyi Cai[a], Yongfeng Mei[c,*], Suwit Kiravittaya[d,*]

[a] Roll Forging Research Institute, Jilin University, 5988 Renmin Street, Changchun 130025, China
[b] National Laboratory for Infrared Physics, Shanghai Institute of Technical Physics, Chinese Academy of Sciences, 500 Yutian Road, Shanghai 200083, China
[c] Department of Materials Science, Fudan University, 220 Handan Road, Shanghai 200433, China
[d] Advanced Optical Technology Laboratory, Department of Electrical and Computer Engineering, Faculty of Engineering, Naresuan University, Taphoo, Muang, Phitsanulok 65000, Thailand

ABSTRACT

Optical modes in axially asymmetric microtube resonators made by dielectric materials are calculated by means of a semi-analytical approach. The Helmholtz equation for the microtube resonators can be separately solved by decomposing the mode field profile into two parts, i.e., cross-section plane and axial direction. Effective refractive index theory is used to link between the above two parts. Analytic axial fields can be approximated by Airy functions while conventional whispering-gallery mode fields written in term of Bessel functions are characteristics of the field in the cross-section plane. The validity of the semi-analytical formulation is confirmed by comparing with finite element simulations.

1. Introduction

Optical resonators (or cavities) are interesting structures, which confine light in three dimensions (3D) for both fundamental properties and engineering applications [1–5]. For instance, the quantum efficiency of single photon devices can be enhanced when the light source is placed into a resonator [4]. Moreover, conventional lasers (e.g., the gas, solid state, and semiconductor lasers) must contain at least one resonator configuration [5]. Among high-quality optical resonators, whispering-gallery mode (WGM) resonators have gained much attention [2,6]. Conventional WGM resonators for confining light in visible-to-near infrared ranges are microdisks (Fig. 1(a)), microrings (Fig. 1(b)), and microspheres (Fig. 1(c)) [2]. Each structure has its own advantages, which can be utilized in any specific designs or applications. Microtubes (Fig. 1(d)), which are relatively new WGM resonators [7–11], have many potential applications especially in optofluidics [12] due to their integratable capability into the micro-fluidic channel structure [13]. Similar to microdisks and microrings, a strong light confinement in microtube resonators originates from the total internal reflection along the outer curved surface, as shown in Fig. 1. In contrast, the axial confinement of light in the microtube resonators is typically weak and produces higher order modes for each azimuthal mode [9,14–17]. For an axially symmetric confinement, the light field will be localized in the middle [9,14]. However, for some realized microtube resonators [15,18], the axial confinement is asymmetric. Therefore, the localized light field is not in the middle. Experimental findings of this asymmetric confined light field have been reported [15]. Later, nontrivial optical phenomena (i.e., Berry phase and spin-orbit coupling of light) have been observed in the asymmetric microtube resonators [18]. However, analytic optical fields for the asymmetric microtube resonators have not been investigated/developed so far.

In this work, we theoretically investigate the axially asymmetric property of microtube resonators. In experiments, the asymmetry can be due to the change of microtube's wall thickness and/or its diameter [9,14,15,13]. However, we maintain a perfect tubular structure with a circular cross-section in our consideration here. Analytical field profiles in terms of Airy, Bessel and Hankel functions can thus be obtained for the confinements of light in axial direction and cross-section plane. From this calculation, we can semi-analytically characterize the spatial properties of both electric and magnetic fields in the axially asymmetric microtube resonators. The calculated results agree well with those of the simulations. These results will help with the understanding of the light confinement in symmetric/asymmetric microtube resonators.

2. Formulation

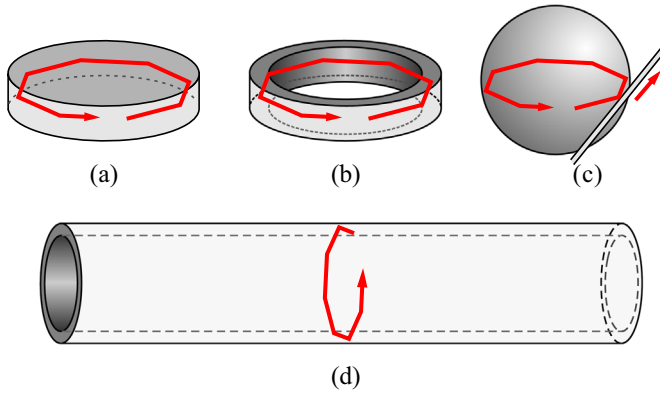Schematic illustration of axially asymmetric microtube resonators

Fig. 1. Schematics of (a) microdisk, (b) microring, (c) microsphere (with a coupled fiber) and (d) microtube resonators. Ray representation of WGM fields is shown as solid red lines in the structure. (For interpretation of the references to color in this figure legend, the reader is referred to the web version of this article.)

with relevant parameters is shown in Fig. 2. In Fig. 2(a), two refractive indices n_1 and n_2 are introduced. Three geometrical parameters, i.e., the length L of a microtube, its inner and outer radii R_1 and R_2, are defined in Fig. 2(a) and (b). According to the structural symmetry, cylindrical coordinate (ρ, ϕ, z) is used throughout this work. For the microtube resonators, the refractive index $n(r)$ of the whole domain is a function of radial and axial coordinates (ρ and z), i.e., $n(r) = n(\rho, z)$, which can be written as

$$n(\rho, z) = \begin{cases} n(z), & R_1 \le \rho \le R_2 \bigcap 0 \le z \le L, \\ n_0 = 1, & \text{otherwise} \end{cases} \tag{1}$$

where $n(z) = n_1 + (n_2 - n_1)z/L$ and n_0 is the refractive index of the microtube's environment, which is assumed to be one (for vacuum or air environment). Dispersion-free (frequency-independent) property is considered for the microtube's wall material.
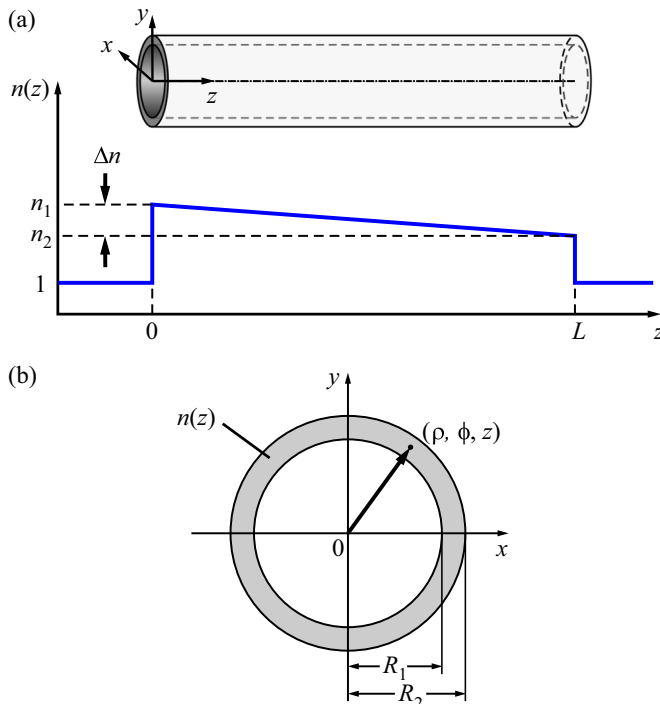

Fig. 2. (a) Axially asymmetric refractive index profile along the axial direction (z-axis) and (b) refractive index profile on a cross-section plane (xy-plane) of microtube resonators. Relevant parameters are defined in the main text.

2.1. Helmholtz equation

We start our formulation with the well-known scalar Helmholtz equation:

$$\nabla^2 F(r) + n^2(r)k^2 F(r) = 0, \tag{2}$$

where $\nabla^2 = \nabla^2_{3D} = \nabla^2_{2D} + \partial^2/\partial z^2$ is the 3D Laplacian operator, $\nabla^2_{2D} = \frac{1}{\rho}\frac{\partial}{\partial \rho}(\rho\frac{\partial}{\partial \rho}) + \frac{1}{\rho^2}\frac{\partial^2}{\partial \phi^2}$ is the two-dimensional (2D) Laplacian operator, $F(r)$ is a scalar field function which is a component of electric field E or magnetic field H, and $k = \omega/c = 2\pi f/c = 2\pi/\lambda$ is the wavenumber where ω is the angular frequency, c is the speed of light in vacuum, f is the temporal frequency, and λ is the free space wavelength. Note that $n(r)$ and $F(r)$ are the input and output functions of this problem.

2.2. Separation of variables

Eq. (2) is a second-order partial differential equation, which can be solved by several mathematical techniques. Here, we apply the method of separation of variables [19], i.e.,

$$F(\rho, \phi, z) = \Phi(\rho, \phi)\Psi(z). \tag{3}$$

Putting Eq. (3) into Eq. (2) and dividing it by $\Phi(\rho, \phi)\Psi(z)$ we have

$$\frac{1}{\Phi(\rho, \phi)}\nabla^2_{2D}\Phi(\rho, \phi) + \frac{1}{\Psi(z)}\frac{d^2\Psi(z)}{dz^2} + n^2k^2 = 0. \tag{4}$$

By using an effective refractive index theory for the axial confinement [20], we can assume that

$$\frac{1}{\Psi(z)}\frac{d^2\Psi(z)}{dz^2} + n^2k^2 = n^2_{eff}k^2, \tag{5}$$

where n^2_{eff} is the refractive index due to the axial confinement. Then, we have two differential equations, which can be separately solved. They are

$$-\frac{d^2\Psi(z)}{dz^2} + (1 - n^2)k^2\Psi(z) = (1 - n^2_{eff})k^2\Psi(z), \tag{6}$$

and

$$\nabla^2_{2D}\Phi(\rho, \phi) + n^2_{eff}k^2\Phi(\rho, \phi) = 0. \tag{7}$$

Note that $k^2\Psi(z)$ is added into both sides of Eq. (6) in order to make a kind of Schrödinger-like equation and solve it with standard methods in Quantum Mechanics [21]. There is another possible treatment for Eq. (2) [7,9,14], which is done by decomposing k into k_{circ} and k_z ($k^2 = k^2_{circ} + k^2_z$) and then formulating another kind of Schrödinger-like equation.

2.3. Axial field profile

For the axial confinement, Eq. (6) must be solved. This is an eigenvalue problem similar to a finite square well problem in Quantum Mechanics [22,21,23] ($\hbar^2/2m$ is set to be 1.). If one uses an infinite square well approximation for the *symmetric* case, i.e., $n_2 = n_1 \gg n_0 = 1$, the analytical solution is

$$\Psi(z) = \begin{cases} \sin(\frac{l\pi z}{L}), & 0 \le z \le L, \\ 0, & \text{otherwise} \end{cases} \tag{8}$$

where $l = 1, 2, 3, \dots$ is the axial mode index. Substituting Eq. (8) into Eq. (6), one obtains

$$n_{eff,l} = \sqrt{n_1^2 - (\frac{l\pi}{kL})^2}. \tag{9}$$

This effective refractive index is used for solving Eq. (7) and finding the wavenumber k (eigenvalue) at corresponding axial mode l. Note that if $kL \gg l\pi$, the effective refractive index can be well approximated by n_1 and

this means that there is only a weak axial confinement in the microtube resonators.

For *asymmetric* case, we assume $n_0 = 1 \ll n_2 < n_1$. The confinement potential in Eq. (6) is

$$(1 - n^2)k^2 = (1 - (n_1 + (n_2 - n_1)\frac{z}{L})^2)k^2 \qquad (10)$$

$$\approx (1 - n_1^2 + 2n_1(n_1 - n_2)\frac{z}{L})k^2. \qquad (11)$$

Linearization of Eqs. (10) and (11) is possible since we consider only the small difference between n_1 and n_2 ($|\Delta n| = |n_1 - n_2| \ll n_1$). This condition is probably valid for microtubes made by compound materials such as $Al_xGa_{1-x}As$ with graded variation of its content. Without this linearization, the general nonlinear refractive index profile might be considered. However, there is no such a general solution of the nonlinear refractive index profile for this problem Eq. (6). For the linear profile, if $n_1 > n_2$, the confinement potential is linearly increased with z. When an infinite well approximation is used, the analytical solution of Eq. (6) can be written in term of Airy Ai functions [22,21,23]. That is

$$\Psi(z) = \begin{cases} \text{Ai}\left(\dfrac{a + bz/L}{(b/L)^{2/3}}\right), & 0 \le z \le L, \\ 0, & \text{otherwise} \end{cases} \qquad (12)$$

where $a = (1 - n_1^2)k^2 - (1 - n_{eff}^2)k^2 = (n_{eff}^2 - n_1^2)k^2 < 0$ and $b = 2n_1(n_1 - n_2)k^2$. The effective refractive index n_{eff} (in a) can numerically be obtained by applying the boundary conditions $\Psi(z = 0) = \Psi(z = L) = 0$.

2.4. Cross-sectional field profile

For the perfect ring geometry shown in Fig. 2(b), WGM field profile is expected as the solution of Eq. (7). For this solution, we can decompose $\Phi(\rho, \phi)$ into $f(\rho)e^{\pm jm\phi}$ where $j = \sqrt{-1}$ and m is the azimuthal mode index. Eq. (7) can then be further decomposed. The solution for the differential equation in radial direction is

$$f(\rho) = \begin{cases} C_1 J_m(k\rho), & 0 \le \rho < R_1 \\ C_2 J_m(n_{eff}k\rho) + C_3 Y_m(n_{eff}k\rho), & R_1 \le \rho \le R_2, \\ C_4 H_m^{(1)}(k\rho), & \rho > R_2 \end{cases} \qquad (13)$$

where $J_m(.)$ and $Y_m(.)$ are the Bessel function of the first and second kinds, $H_m^{(1)}(.)$ is the Hankel function of the first kind [3], and C_1, C_2, C_3 and C_4 are constants obtained by matching the boundary conditions of the considered fields at the inner and outer interfaces.

For calculating possible cross-sectional field profiles, one can classify them as either transverse magnetic (TM) or transverse electric (TE) modes [3]. The two modes have distinct characteristics due to the different applicable boundary conditions. For TM modes, the considered field in Eq. (2) is E_z ($F = E_z$) while it is H_z for TE modes. Once the specific fields (E and H) at domain boundaries are matched, non-zero C_1, C_2, C_3 and C_4 are obtained only at specific m and k. Obtained k values are the eigenvalues of the problem.

3. Numerical results

Formulation presented in the former section can be visualized by considering a specific microtube geometry. For instance, we consider a $10 - \mu m$-long microtube made by semiconductor materials (i.e., AlGaAs) operating at near infrared wavelength range ($n_{AlGaAs}=3.3-3.4$ at $k=5 \mu m^{-1}$) [24]. Inner and outer radii of the microtube are set to be $0.8 \mu m$ and $1.0 \mu m$, respectively.

Fig. 3(a) shows the results from the numerical calculation of the n_{eff} when an asymmetric potential is introduced via $\Delta n = n_1 - n_2$. By increasing Δn, n_{eff} for each axial mode l decreases. For each mode, a linear relation between n_{eff} and Δn can be assumed. For $\Delta n \approx 0$ ($=10^{-5}$), the numerically calculated n_{eff} can be well fitted with the
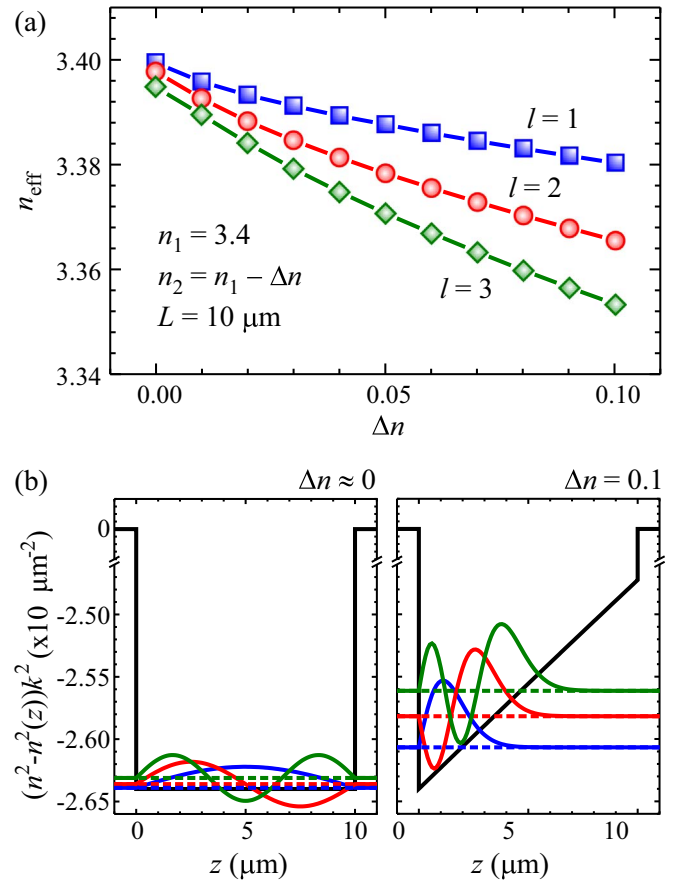

Fig. 3. (a) Calculated n_{eff} for the first three confined modes (l=1, 2, and 3) as a function of Δn. (b) Potential and the first three calculated axial field profiles when $\Delta n \approx 0$ (left) and $\Delta n = 0.1$ (right). Dashed lines are calculated $(1 - n_{eff,l}^2)k^2$ of each mode.

analytically calculated one Eq. (9).

Fig. 3(b) shows the confinement potential and the axial field profiles for the first three confined modes (l=1, 2, and 3). The nearly sinusoidal field profile is obtained from Airy function when $\Delta n \approx 0$ in the left side of Fig. 3(b). For the large Δn, well-separated field profiles are obtained. Characteristic feature of asymmetric Airy function is observed as well. By adjusting the degree of asymmetry, one can vary the spatial distribution of the field profiles. This controllability might be very useful when specific objects (e.g., nanoparticles, quantum dots, or molecules) are designed to couple with the optical field in the resonator [1,2].

For the cross-sectional field profile, WGMs are obtained. Searching for the solutions (eigenvalues) at $k \approx 5 \mu m^{-1}$ and $n_{eff} = 3.4$, we found TM modes with m=11, 12, and 13 at k=4.4503, 4.7629, and 5.0742 μm^{-1}, respectively. Fig. 4(a) shows the TM mode (E_z) profile with m=12. This field has continuity for both value and slope at the inner and outer walls of the microtube. For TE modes, the WGM field
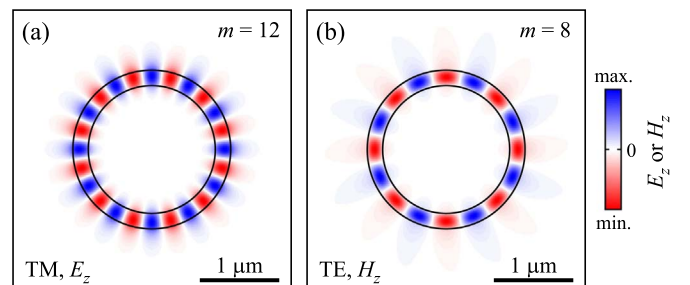

Fig. 4. Cross-sectional field profiles for (a) TM mode (E_z) with m=12 and (b) TE mode (H_z) with m=8. See text for calculation parameters.

profiles with a lower mode index are obtained at k=4.6255, 4.8774, and 5.115 μm^{-1} for m=7, 8, and 9, respectively. Fig. 4(b) shows the TE mode (H_z) with m=8. This field has continuous value across the boundary but the slope is discontinuous due to the applied boundary conditions [3].

To complete our numerical demonstration, we plot 3D field profiles for the cases of symmetric and asymmetric potentials for the first three axial modes in Fig. 5. Isosurfaces with the value of 0.25 and 0.5 of the maximum values are presented. Figs. 5(a)–(c) show symmetric optical fields, which are distributed in the whole microtube. In contrast, optical fields in axially asymmetric microtube (Figs. 5(d)–(f)) are localized in the high refractive index area [25].

4. Simulation comparison

Simulations using finite element method (FEM) [26–28] are fulfilled in this section to confirm the validity of the formulation developed above. For the simulations, we generate axially asymmetric microtube structure (inner radius=0.8 μm, outer radius=1.0 μm, and 10 μm long) in a 3D simulation domain covered by the Perfectly Matched Layer (PML). Then tetragonal meshes are generated based on this structure. By numerically solve/search for eigenvalues near initial wavenumber $k = 5$ μm^{-1} of the vectorial Helmholtz equation, we can confidently obtain the solutions, which are eigenmode and 3D mode field profile. Fig. 6 shows the simulated wavenumbers together with those from analytical calculations based on the formulation. For the simulation results, one cannot define TE or TM modes because they are coupled and the coupling is involved in the simulations. Instead, we label them as TE-like or TM-like modes.

Overall speaking, a good agreement between the FEM simulations and analytical calculations is obtained. It is indicated that coupling between TE and TM modes is generally weak so that it can be ignored in the formulation. However, it is stronger for TE modes with a smaller azimuthal mode index, which results in a relatively bigger deviation from simulations (see the left of Fig. 6). The stronger coupling is due to their larger evanescent field in the environment [29], where external coupling between the dynamics of the axial and the cross-sectional propagations of light is stronger [14]. External coupling has been used to obtain high-quality optical modes [30,31], and we might investigate it in our future works. Nevertheless, these results show that the formulation presented in this work would be useful to obtain resonant modes for axially asymmetric microtube resonators with a certain precision.
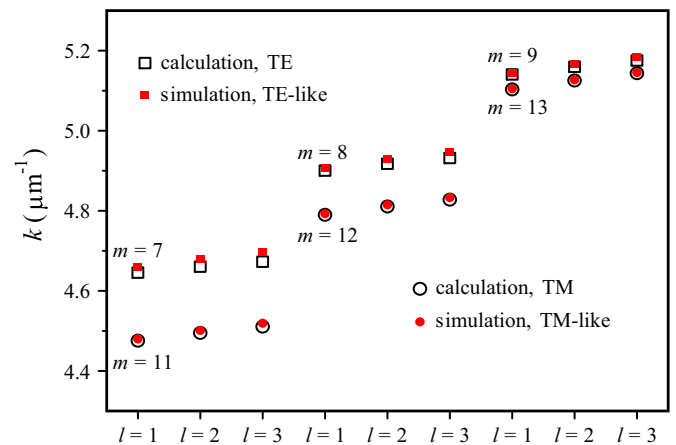
Fig. 5. 3D TM mode field profiles in the cases of axially symmetric ((a), (b) and (c)) and axially asymmetric ((d), (e) and (f)) potentials for Δn=0.1, l=1, 2, and 3, and m=12.

Fig. 6. Comparison between FEM simulations and analytical calculations with Δn=0.1.

By comparing the semi-analytical approach presented in this work and the FEM, we found that the semi-analytical method allows us to theoretically estimate the maximum field density as well as the spread of the field (by the analysis of $\Psi(z)$ shown in the Eq. (12). Moreover, one can use the Eq. (12) to obtain the effective refractive index from the axial confinement by applying the boundary conditions. By applying this model (for perfect circular tubes), one does need only numerical root findings. However, for such a rolled-up tube resonator [7–11], where circular symmetry is broken, 2D FEM can be applied along with the model proposed in this work to calculate 3D mode profile and eigenmode instead of a full 3D FEM simulation.

5. Conclusion

We develop semi-analytical formula for the field profiles of optical modes in axially asymmetric microtube resonators. By applying separation of variables to Helmholtz equation and adopting effective refractive index theory, the function for an analytic field profile in the axial direction can be written as an Airy function. For the cross-sectional field profile, typical whispering-gallery modes are obtained. The good agreement between the simulations and the analytical calculations confirms the validity of the semi-analytical formula. This work will enhance an engineering of confined optical field, which is crucial for developing novel optical micro-/nano-devices.

References

[1] C. Weisbuch, H. Benisty, R. Houdré, Overview of fundamentals and applications of electrons, excitons and photons in confined structures, J. Lumin. 85 (2000) 271.
[2] K.J. Vahala, Optical microcavities, Nature 424 (2003) 839.
[3] C.A. Balanis, Advanced Engineering Electromagnetics, Wiley, New York, 1989.
[4] C. Santori, D. Fattal, Y. Yamamoto, Single-Photon Devices and Applications, Wiley, New York, 2010.
[5] W.S.C. Chang, Principles of Lasers and Optics, Cambridge University Press, New York, 2005.
[6] X.-F. Jiang, C.-L. Zou, L. Wang, Q. Gong, Y.-F. Xiao, Whispering-gallery micro-cavities with unidirectional laser emission, Laser Photonics Rev. 10 (2016) 40.
[7] T. Kipp, H. Welsch, C. Strelow, C. Heyn, D. Heitmann, Optical modes in semiconductor microtube ring resonators, Phys. Rev. Lett. 96 (2006) 077403.
[8] R. Songmuang, A. Rastelli, S. Mendach, O.G. Schmidt, SiOx/Si radial superlattices and microtube optical ring resonators, Appl. Phys. Lett. 90 (2007) 091905.
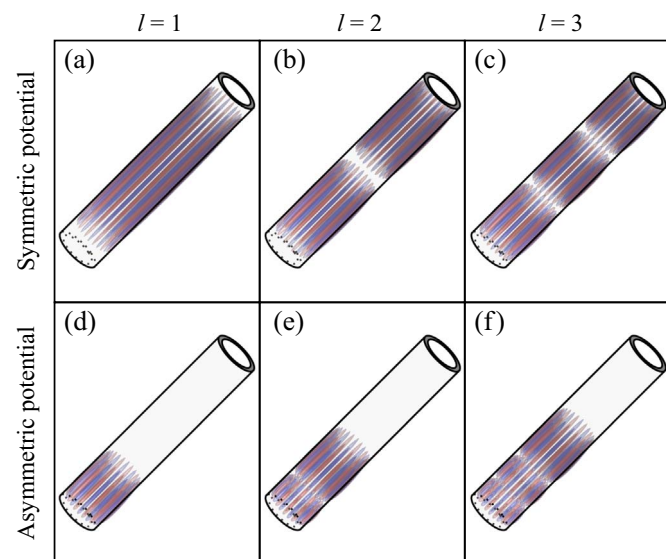
[9] C. Strelow, H. Rehberg, C.M. Schultz, H. Welsch, C. Heyn, D. Heitmann, T. Kipp, Optical microcavities formed by semiconductor microtubes using a bottlelike geometry, Phys. Rev. Lett. 101 (2008) 127403.

[10] J. Wang, T. Zhan, G. Huang, P.K. Chu, Y. Mei, Optical microcavities with tubular geometry: properties and applications, Laser Photonics Rev. 8 (2014) 521–547.

[11] S. Sedaghat, A. Zarifkar, Evanescent coupling of asymmetric self-rolled-up microtube and slab waveguide, Opt. Commun. 382 (2017) 167.

[12] Y. Chen, F. Yu, C. Yang, J. Song, L. Tang, M. Li, J.-J. He, Label-free biosensing using cascaded double-microring resonators integrated with microfluidic channels, Opt. Commun. 344 (2015) 129.

[13] S.M. Harazim, V.A.B. Quiñones, S. Kiravittaya, S. Sanchez, O.G. Schmidt, Lab-in-a-tube: on-chip integration of glass optofluidic ring resonators for label-free sensing applications, Lab Chip 12 (2012) 2649.

[14] C. Strelow, C.M. Schultz, H. Rehberg, M. Sauer, H. Welsch, A. Stemmann, C. Heyn, D. Heitmann, T. Kipp, Light confinement and mode splitting in rolled-up semiconductor microtube bottle resonators, Phys. Rev. B 85 (2012) 155329.

[15] V.A.B. Quiñones, L. Ma, S. Li, M.R. Jorgensen, S. Kiravittaya, O.G. Schmidt, Enhanced optical axial confinement in asymmetric microtube cavities rolled up from circular-shaped nanomembranes, Opt. Lett. 37 (2012) 4284.

[16] S. Li, L. Ma, H. Zhen, M.R. Jorgensen, S. Kiravittaya, O.G. Schmidt, Dynamic axial mode tuning in a rolled-up optical microcavity, Appl. Phys. Lett. 101 (2012) 231106.

[17] S. Böttner, S. Li, M.R. Jorgensen, O.G. Schmidt, Polarization resolved spatial near-field mapping of optical modes in an on-chip rolled-up bottle microcavity, Appl. Phys. Lett. 105 (2014) 121106.

[18] L. Ma, S. Li, V.M. Fomin, M. Hentschel, J.B. Götte, Y. Yin, M.R. Jorgensen, O.G. Schmidt, Spin-orbit coupling of light in asymmetric microcavities, Nat. Commun. 7 (2016) 10983.

[19] S. Li, L. Ma, S. Böttner, Y. Mei, M.R. Jorgensen, S. Kiravittaya, O.G. Schmidt, Angular position detection of single nanoparticles on rolled-up optical microcavities with lifted degeneracy, Phys. Rev. A 88 (2013) 033833.

[20] P. Yeh, Optical Waves in Layered Media, Wiley, New York, 2005.

[21] J.H. Davies, The Physics of Low-Dimensional Semiconductors: an Introduction, Cambridge University Press, New York, 1998.

[22] D.J. Griffiths, Introduction to Quantum Mechanics, Prentice Hall, Englewood Cliffs, New Jersey, 1995.

[23] E. Merzbacher, Quantum Mechanics, Wiley, New York, 1998.

[24] S. Adachi, GaAs, AlAs, and AlxGa1xAs: material parameters for use in research and device applications, J. Appl. Phys. 58 (1985) R1.

[25] X. Lin, W. Fang, Localized high-Q modes in conical microcavities, Opt. Commun. 381 (2016) 169.

[26] Y. Fang, S. Li, Y. Mei, Modulation of high quality factors in rolled-up microcavities, Phys. Rev. A 94 (2016) 033804.

[27] Y. Yin, S. Li, V. Engemaier, S. Giudicatti, E. Saei Ghareh Naz, L. Ma, O.G. Schmidt, Hybridization of photon-plasmon modes in metal-coated microtubular cavities, Phys. Rev. A 94 (2016) 013832.

[28] Y. Yin, S. Li, S. Böttner, F. Yuan, S. Giudicatti, E. Saei Ghareh Naz, L. Ma, O.G. Schmidt, Localized surface plasmons selectively coupled to resonant light in tubular microcavities, Phys. Rev. Lett. 116 (2016) 253904.

[29] J. Trommer, S. Böttner, S. Li, S. Kiravittaya, M.R. Jorgensen, O.G. Schmidt, Observation of higher order radial modes in atomic layer deposition reinforced rolled-up microtube ring resonators, Opt. Lett. 39 (2014) 6335.

[30] J. Wiersig, Formation of long-lived, scarlike modes near avoided resonance crossings in optical microcavities, Phys. Rev. Lett. 97 (2006) 253901.

[31] Q.H. Song, H. Cao, Improving optical confinement in nanostructures via external mode coupling, Phys. Rev. Lett. 105 (2010) 053902.